Effect of water content on the constitutive response of a cellulose foam

Lizi Cheng[a], Vikram Deshpande[a], Norman Fleck[a,*]

Department of Engineering, University of Cambridge, Cambridge CB2 1PZ, UK

31 March 2023

Abstract

Cellulose foams can undergo a large one-way actuation strain when taken from a dry, pre-compressed state to a damp state by the addition of water. In order to develop a predictive capability for the 3D actuation of a foam-based structure with a non-uniform water concentration it is first necessary to understand the mechanical properties of the foam (including actuation strain) as a function of water content. Here, we report the anisotropic constitutive response of a cellulose foam as a function of water content. Over the range of strain rate and water content considered, the cellulose foam is adequately approximated by a visco-plastic, transversely isotropic, compressible constitutive model. Unloading from the plastic state by a stress drop equal to the initial yield stress leads to reversed plastic flow: this is an extreme form of kinematic hardening.

Key words

cellulose foams, anisotropy, constitutive model, soft solid, actuation strain, non-linear kinematic hardening

1. Introduction

Cellulose is the most ubiquitous organic solid, yet there remains only a limited understanding of its mechanical response, particularly in the presence of moisture, Kadla et al. (2000). Many measurements have been made of the uniaxial properties of natural cellulose foams in the form of wood (Ashby and Gibson, 1997; Dinwoodie, 2000). The axial properties such as modulus and strength scale linearly with relative density, while the transverse properties depend upon relative density in a non-linear manner. Hence, species of wood that are of low relative density, such as balsa, are highly anosotropic (Tagarielli et al. 2005). Cellulose foams are derived from wood fibres and consequently they are environmentally more friendly than polymeric foams. Additionally, the tunable mechanical properties of cellulose foams, along with their biocompatibility, endow them with broad applications in biomedicine, such as wound dressing, tissue regeneration, repair, and healing (Lin and Dufresne, 2014). Whilst the mechanics of lightweight and porous foams have attracted considerable recent interest (Ashby et al., 2000; Deshpande and Fleck, 2001) much less is known about the mechanical response of cellulose-based foams, and their dependence upon the degree of hydration (Ha et al., 2018; Kim et al., 2017). Cellulose foams can swell considerably by the addition of water (Yamamoto et al., 2001), and the imbibition of water into dry cellulose gives an additional degree of freedom to the response of this class of solid foams (Das et al., 2022; Mirzajanzadeh et al., 2019).

Cellulose has a strong affinity for water due to its many hydroxyl groups (KADLA and GILBERT, 2000). The main structural units of natural and artificial cellulose are microfibrils in the form of ordered assemblies of polymeric chains. Typically, the microfibrils are of length on the order of tens of micrometres, and widths on the order of tens of nanometres. Recently, (Chen et al., 2022) have performed molecular dynamics

simulations to show that water molecules migrate to the microfibril-microfibril interfaces in cellulose fibril aggregates to form weak confined water layers. These calculations support previous first principles calculations by (Sinko and Keten, 2014) and confirm that the presence of a water layer facilitates interfibril shear deformation. Consequently, the modulus and strength of the cellulose fibrils (comprising many microfibrils) are reduced. A mixture theory could be used to determine the macroscopic effective properties of the fibrils within the porous cell walls of the cellulose foam, but there is additional structural hierarchy to consider in order to determine the relation between cell wall properties and macroscopic foam response.

A literature has emerged on the multi-axial yield response of isotropic polymeric foams (Deshpande and Fleck, 2000). (Tjahjanto et al., 2015) have developed a multi-axial visco-plastic model for the anisotropic mechanical response of cellulose materials such as high density paper-board, along with experimental support. But there remains a lack of knowledge of, and understanding for, the sensitivity of the mechanical behaviour of these materials to water content.

Cellulose-based moisture actuators can be used in soft robotics applications such as grippers, arms, smart switches, and artificial muscles (Zhu et al., 2018), as well as in biomedical devices (Nan et al., 2019) and the electronic industry (Lv et al., 2021). The actuation of dry pre-compressed foam requires the time-dependent imbibition of water into the foam by some combination of diffusion and capillary flow, and time-dependent expansion of the foam. The current study is not concerned with the details of such a transient response; it is recognised, however that time-dependence is of clear significance if the transient response of a deployable structure is relevant to a particular application.

The present investigation makes use of the same cellulose foam as that used by

(Das et al., 2022; Mirzajanzadeh et al., 2019, 2020) in their recent water imbibation studies. However, the present aim is different: we shall characterize the microstructure and uniaxial response as a function of water content and rate of loading. This mechanical understanding provides the experimental foundation for future experimental and theoretical studies on foam actuation. Preliminary studies by Mirzajanzadeh et al. (2019, 2020) show that a pre-compressed foam can undergo a one-way, unidirectional actuation with a change in length by a factor of about 10 when taken from the dry state (Fig. 1(a)) to the damp state (Fig. 1(b)). The enormous actuation strain along the so-called rise direction R implies that a lattice made from the foam can be deformed by the addition of water to one strut of the lattice. This is illustrated in Figs. 1 (c) and (d). Dry, pre-actuated foam is cut into the form of a fully-triangulated beam-like lattice of Fig. 1(c). Then, upon adding a small quantity of water to an upper strut, the strut extends along the rise direction R and the lattice distorts, see Fig. 1(d). Preliminary tests suggest that this actuation response is independent of the direction of gravity, in part due to the fact that the mass of water required for actuation is less than that of the dry foam arm that is actuated. However, the actuation is not ideal: although the beam-like lattice rotates about a hinge below the actuated bar, the actuated strut also buckles due to the finite stiffness of the remaining lattice elements. The optimal design of such actuating lattices will require a detailed knowledge of the effect of water content upon the stress-strain response of the foam, thereby motivating the present study.

An analogy exists between the water-induced actuation of a cellulose foam and the thermally-induced shape-memory response of a range of thermoplastics, see for example Zhou et al (2022). A foam made from a shape-memory polymer (SMP) has the capability to be compressed above its glass transition temperature and remain in a temporary shape; upon reheating to a sufficiently high temperature (above the glass

transition temperature) the ‘pre-compressed foam’ recovers its original shape of an expanded foam. The structural memory is due to the presence of entanglements and cross-links, and the ability to remain in the compressed state is due to the freezing of van der Waals bonds between polymer chains.

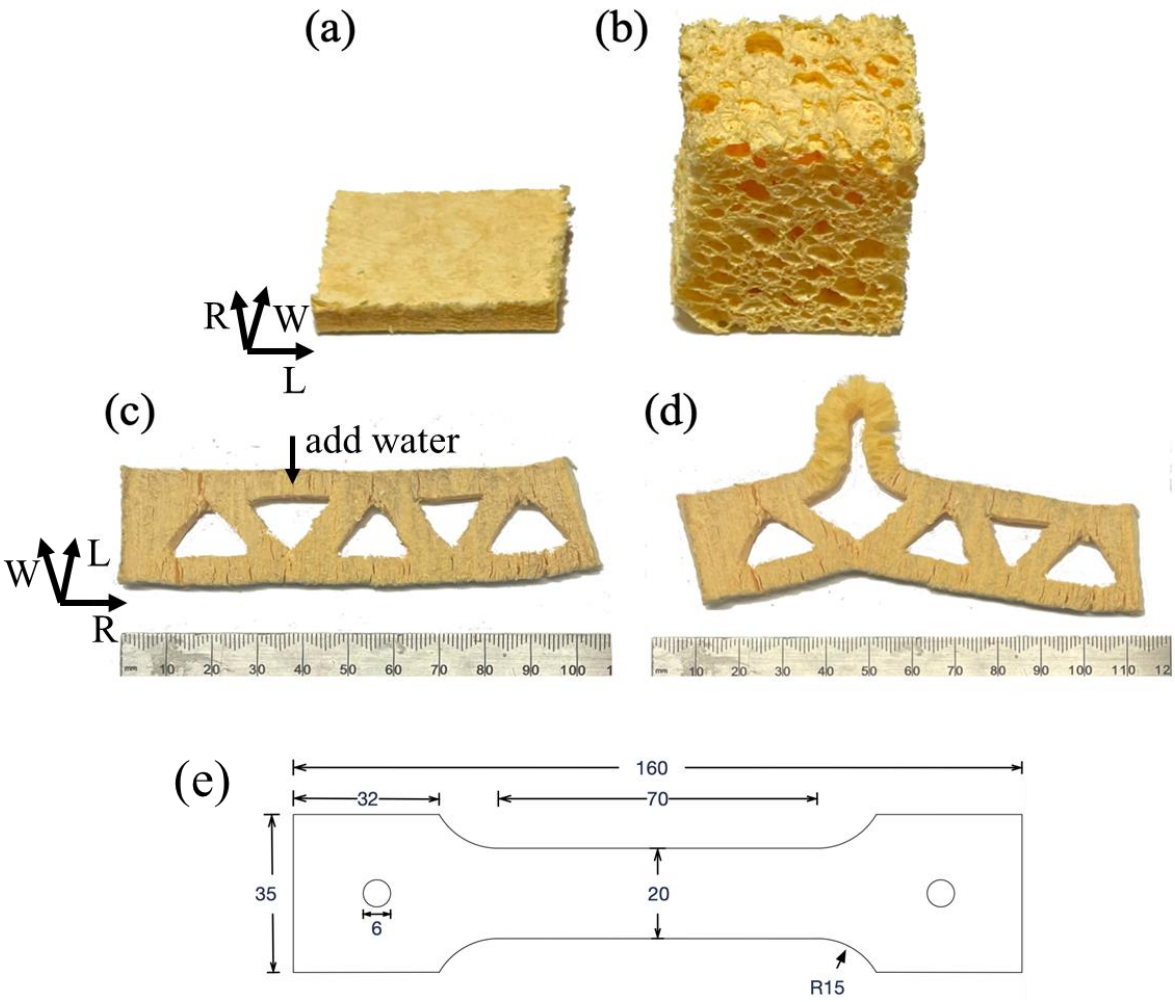

Fig. 1 Optical images of the cellulose foam. (a) Dry foam prior to actuation, of dimension 25×25×2.43 mm^3; (b) Dry fully-expanded foam of dimension 25×25×25 mm^3; (c) A fully triangulated foam lattice in the pre-actuated, pre-compressed state, of overal dimension 110 mm x 25 mm x 5 mm. The lattice is contructed by adhering together (with PVA-based adhesive) a stack of sheets of thickness 2.43mm in the rise, R-direction, and then

cutting a series of triangles to define the shape of the lattice. Water is added to one strut in order to actuate it; (d) Actuated lattice. The actuated strut has buckled. (e) Dogbone tensile specimen of cellulose foam in the fully-expanded state. All dimensions are in mm.

Scope of study

The tensile and compressive responses of an anisotropic cellulose foam in the dry and damp states are measured at selected strain rates and at room temperature. The fully expanded dry state exists in the form of commercial foam sheets, and is taken as the reference, stress-free configuration. The microstructural anisotropy of the cellulose foam is investigated by micro computed tomography (CT) and by a scanning electron microscope (SEM). The macroscopic stress versus strain response is measured for uniaxial compression and tension at selected values of strain rate, and the visco-plastic response is extracted as a function of water content. Unloading tests are performed in order to determine whether the response is recoverable or plastic in nature. Additionally, the shapes of the loading and unloading stress versus strain curves are compared to determine the nature of strain hardening (isotropic versus kinematic).

2. Materials and methods

2.1 Fully-expanded cellulose foam in the dry state

The cellulose foam of the present study is derived from wood pulp and is manufactured[1] by mechanically mixing cellulose fibres and an aqueous solution of

[1] Suvic Products Limited, 3 Brunel Rd., Totton, Southampton SO40 3WX, United Kingdom.

sodium sulphate crystals. The mixture is heated to 90 – 95 °C so that the sodium sulphate crystals dissolve and drain, leaving pores in the foam. The foam is compressed in the wet state, thereby shrinking the macro-voids (as defined by the sodium sulphate crystals) into penny-shaped cracks and is then dried and cooled. The direction of compression aligns with the direction of gravity, and this direction is termed the 'rise direction of the foam'. The foam is referred to as 'pre-compressed' in its final dry state. Upon adding water to the foam in the pre-compressed states it expands progressively back to the 'fully-expanded state'. Microstructural studies (Ha et al., 2018; Mirzajanzadeh et al., 2020) reveal that the addition of water re-inflates the macroscale penny-shaped cracks back to millimentre-scale voids and also expands an additional population of micron-scale voids within the cell walls. The actuation is one-way such that, upon drying the expanded foam, it does not return to the compressed state.

Compression specimens were manufactured as follows. Preforms of square shape 25 mm ×25 mm (in plan view) were cut from dry pre-compressed foam sheet of thickness $h_{pre} = 2.43 \pm 0.06$ mm in the rise direction. Dry, fully-expanded specimens were obtained from these preforms by immersing them in water, allowing them to expand freely and then by drying them in an oven at 40 ^{o}C for 3 hours. The final height of the dry, fully-expanded specimens in the rise direction was 25.0 ± 0.6 mm, thereby generating cubic specimens, as shown in Fig. 1(b). We emphasise that full hydration of the foam from the dry, pre-compressed state to the dry, fully-expanded state by the above operation leads to an expansion in the rise direction by a factor of approximately 10. The precise dimensions of each specimen was measured prior to testing.

2.2 Mechanical characterisation in the dry state

Tensile and compressive tests were performed using a screw-driven test machine and, unless otherwise stated, the tests were carried out at a nominal strain rate of 10^{-3} s^{-1}. Two video cameras were used to view the front and side of each specimen, thereby allowing for digital image correlation (DIC) analysis of the progressive deformation during each test via the open source Ncorr DIC package implemened in MATLAB. In particular, contours of Green-Lagrange strain $\eta = \varepsilon_n + \frac{1}{2}{\varepsilon_n}^2$ are obtained as a function of position $\boldsymbol{X}$ in the reference configuration, and $\varepsilon_n(\boldsymbol{X})$ is the nominal strain distribution. The average nominal strain ε_n is obtained by dividing the cross-head displacement by the original height, while the nominal stress σ_n is calculated by dividing the axial force by the initial cross-sectional area in the usual manner. The Young's modulus E is defined by the initial slope of the compressive stress-strain curve. Three identical tests were performed in three orthogonal directions, viz. the longitudinal (L), width (W) and rise (R) directions to determine the degree of anisotropy in the material. These directions are shown in Fig. 1(b).

A limited set of tensile tests were performed using dogbone specimens, following a previous study on metallic foams (Tankasala et al., 2020) and the Standard ASTM E1820 (2013). The dogbone specimens were of thickness 25 mm, with in-plane dimensions given in Fig. 1(e). The end portions of the dogbone specimens were reinforced by filling the porosity with epoxy (Easy Composites Ltd). This local reinforcement enabled the specimens to be pin-loaded instead of end-clamped, thereby ensuring that no end moment was applied. A non-contacting high-precision optical laser extensometer was used to measure the average axial nominal strain over the gauge length of the dogbone specimens.

An additional manufacturing step was needed in order to perform a tensile test on a dogbone specimen in the rise (R) direction due to the fact that the thickness of the expanded foam sheet (25 mm) is much less than the length of the dogbone specimen (160 mm). To mitigate against this, 6 layers of foam were bonded together in a stack, using PVA-based water-resistant wood adhesive (Everbuild Ltd) prior to machining of the dogbone specimens. The adhesive was sufficiently strong that failure did not occur at the glue line.

2.3 Microstructural characterisation in the dry state

The spatial distribution of foam porosity was measured during in-situ compression tests on the foam in the dry, full-expanded state using X-ray 3D Computer Tomography. The scans were performed using a 50 kV X-ray source, a 134 ms exposure duration, and a spatial resolution of 16.85 μm per voxel unit. VGStudio MAX 2.2 software was used for both reconstruction and analysis. The cross-sectional microstructure of the foam state was also observed using a Scanning Electron Microscope (SEM). To do so, specimens were gold-sputtered to improve conductivity, and the SEM characterisation was performed at an acceleration voltage of 6 kV to minimise electron beam damage.

2.4 Preparation of the fully expanded cellulose foam in the damp state

Water was added to the specimens in a controlled manner by placing specimens in the fully-expanded dry state inside a humidifier at a relative humidity of 99% and temperature of 20^{o}C. The mass of water added to the specimen depended upon the exposure time in the humidifier, and the specimen water content versus time curve was

measured by periodically recording the mass gain of a specimen in the humidifier.

Write (h_0, w_0, l_0) as the initial dimensions of the specimen in the R, W and L directions, respectively, in the fully-expanded dry state. Likewise, (h_1, w_1, l_1) are the dimensions in the damp state at any given water content. Then, the components of nominal swelling strain in the 3 directions are:

$$\varepsilon_0^R = \frac{h_1 - h_0}{h_0}, \quad \varepsilon_0^W = \frac{w_1 - w_0}{w_0} \text{ and } \quad \varepsilon_0^L = \frac{l_1 - l_0}{l_0} \tag{1}$$

Let m_0 denote the mass of the fully-expanded dry specimen and m_1 the mass in the damp state. The non-dimensional water content is defined as $\overline{m} = (m_1 - m_0)/m_0$. Prior to measuring the swelling strain we environmentally conditioned each specimen by placing it in a sealed polyethylene bag for 12 hours to ensure that the water content was spatially uniform. Subsequently, we recorded the swelling strain for any given water content $\overline{m}$. Desiccation of the specimens was prevented during the mechanical tests by wrapping the specimens in a layer of PVC 'food wrap' film; experiments confirmed that the presence of the thin PVC wrap had no effect upon the mechanical response of the damp foam.

3. Results and discussion

3.1 Structural anisotropy

The size, shape and distribution of porosity within the dry, fully expanded foam is inherited from the distribution of sodium sulphate crystals that are present in the cellulose pre-cursor prior to their dissolution. We begin by characterising the structure of the dry and fully expanded cubic specimen of side length 25 mm. Figure 2(a) shows mid-plane CT images in the three directions. The voids are approximately oblate spheroids

aligned with the (L,W, R) directions.

The CT images (Fig. 2(a)) and the SEM images in Figs. 2(b-d) reveal structural hierarchy from the millimetre-scale voids (as defined by the size of the sodium sulphate crystals used in the processing of the foam) down to micron-size pores in the cell walls. The microstructure in the L-W plane resembles a stack of cellulose sheets, see Figs. 2(a) and 2(c). In contrast, sections in the L-R and W-R planes display nanofiber bundles.

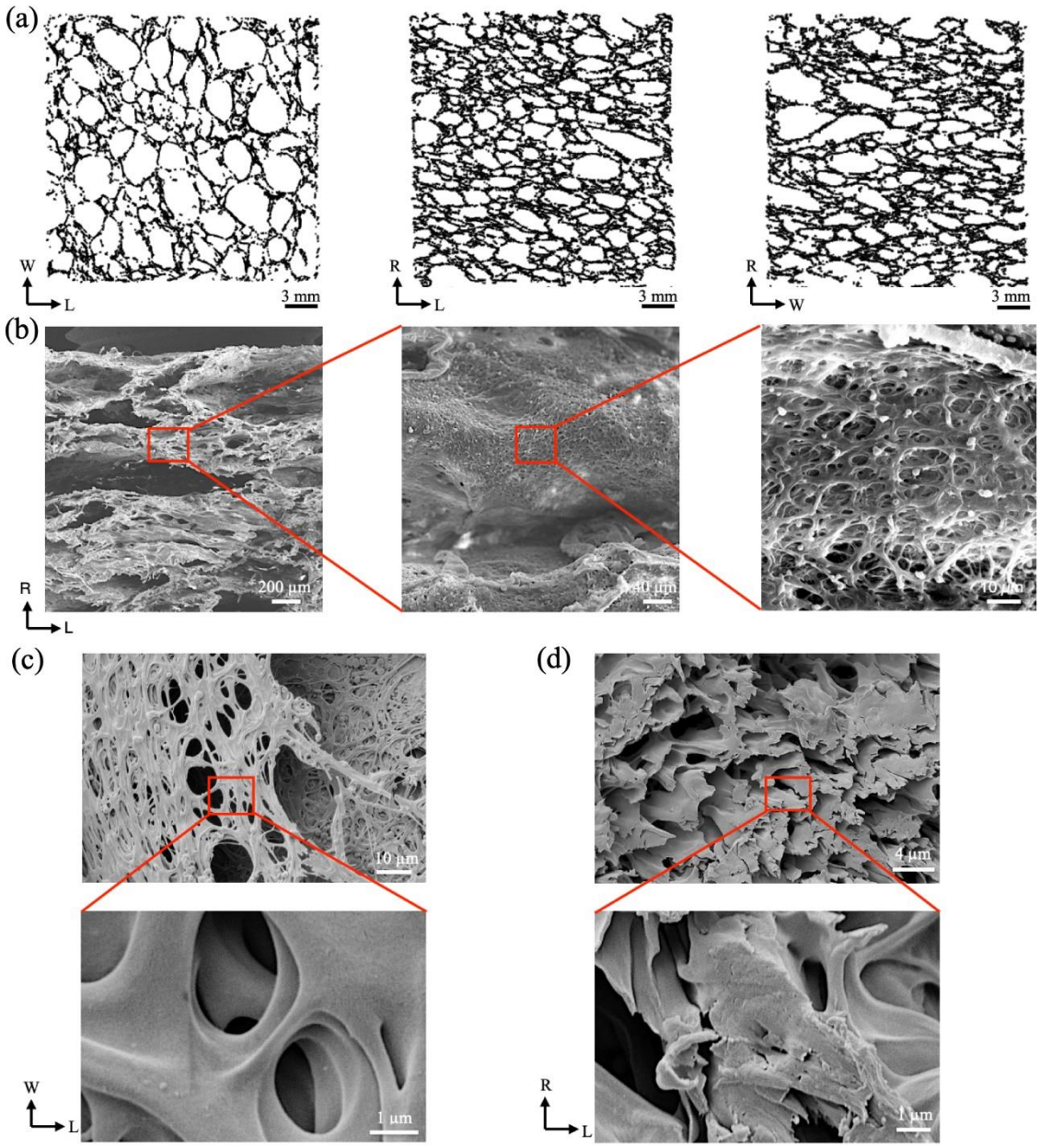

Fig. 2: The anisotropic and hierarchical microstructure of the cellulose foam. (a) Mid-

plane CT images of the three orthogonal W-L, R-L and R-W planes to show that the foams have structural anisotropy similar to that of wood. (b) SEM images of the R-L plane to illustrate the hierarchical structure ranging from the millimetre to nanometre scale. Magnified SEM images of the (c) L-W plane and (d) L-R plane.

3.2 Mechanical characterisation in the dry state

There is choice in the definition of imposed uniaxial strain in the compression and tension tests. We shall employ the nominal strain ε_n measure and take the dry, expanded state as the reference state. Compression tests were performed by placing the cube-shaped specimens between the flat platens of a screw-driven test machine. Write u as the relative axial displacement of the platens imposed at a fixed displacement rate $\dot{u}$. The nominal axial strain components associated with loading in each of the rise (R), width (W) and length (L) directions are definded by

$$\varepsilon_{\mathrm{n}}^{R} = u/h_0, \quad \varepsilon_{\mathrm{n}}^{W} = u/\mathrm{w}_0 \text{ and } \varepsilon_{n}^{L} = u/l_0 \ . \tag{2}$$

Tensile tests were performed on dogbone specimens made from the foam in the dry expanded state, with nominal strain again defined by (2), but the reference lengths (h_0, w_0, l_0) now equal to the gauge length of 50 mm. The extension u of the dogbone specimens was measured using a laser guage, with reflective tabs of the laser system adhered to the specimen and used to define the initial gauge length.

Representative compressive responses in the L,W and R directions are compared in Fig. 3 (a). Each curve is shown by a solid line, with the thickness of the indicating the scatter in response. The L direction is the strongest, while the R direction is the weakest. The deformation mode is made clear from DIC measurements at a compressive nominal

strain of -0.6, see Fig. 3(c): a stable strain hardening response is observed for loading along the softest, R-direction.) The DIC measurements give the Green-Lagrange strain $\eta = \varepsilon_n + \frac{1}{2}{\varepsilon_n}^2$ at an imposed strain $|\varepsilon_n|$=0.6 for compressive loading along the R direction. The tensile response of dry fully-expanded cellulose foam is included in Fig. 3(b). Consistently, the tensile response is stronger than the compressive response and the tensile failure strain equals 0.048 in the L and W directions, and equals 0.192 in the R direction. These contrasting behaviours are rationalised as follows. The compressive response is dominated by cell wall buckling; under tensile loading cell wall bending occurs and this is followed by stretching and ultimately macroscopic tearing (Fleck et al., 2010).

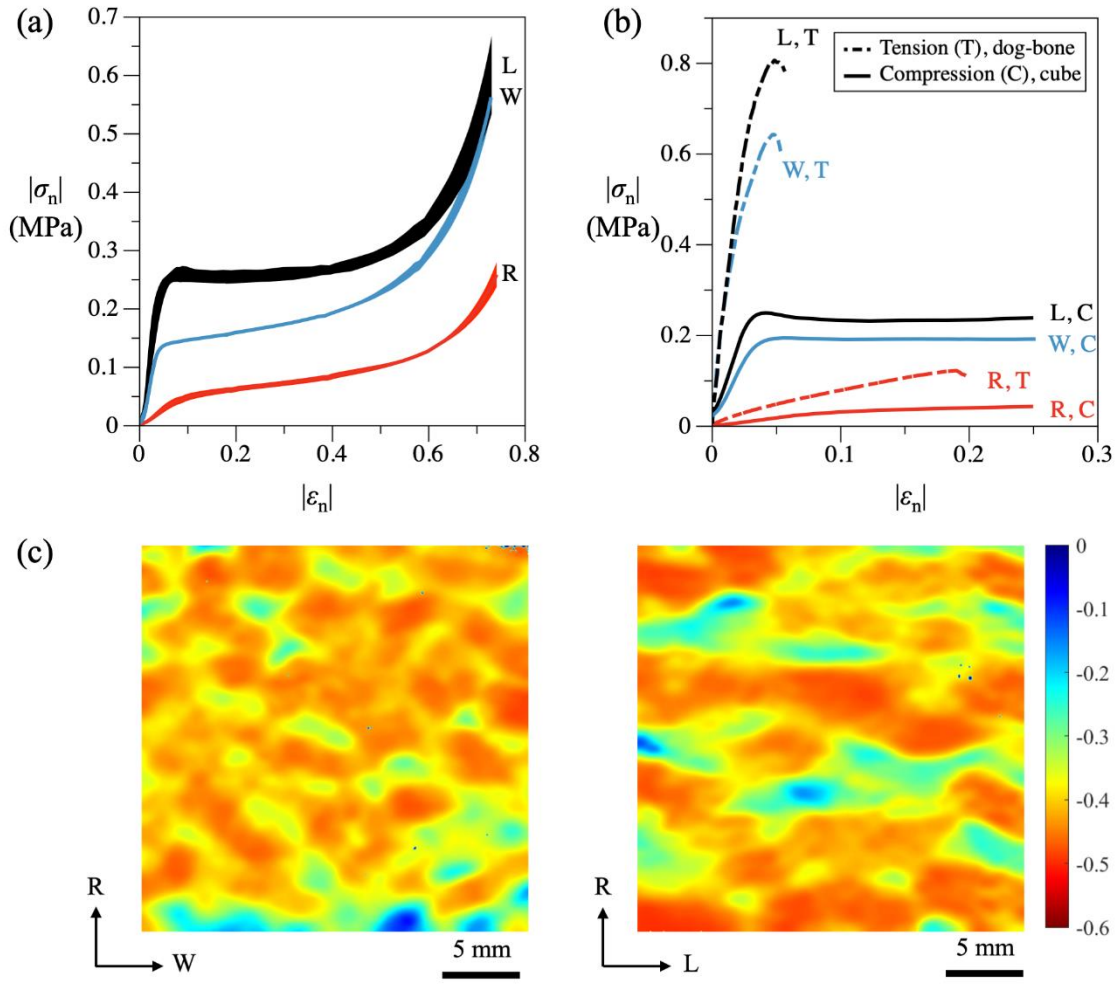

Fig. 3: Nominal uniaxial tensile and compressive responses of the dry and fully-expanded cellulose foam at a strain rate of 10^{-3} s^{-1}. (a) Compressive response in the R, L and W directions, with scatter over three tests displayed by the thickness of the line for each loading direction. (b) Comparison of the compressive (C) and tensile (T) responses of the dry and fully-expanded foams in the R, L and W directions. (c) DIC measurements of the distributions of the Green-Lagrange strain $\eta = \varepsilon_n + \frac{1}{2}{\varepsilon_n}^2$ at an imposed strain $|\varepsilon_n|$=0.6 for compressive loading along the R direction. The measurements are shown on the surfaces of the cubic specimens on the W-R and L-R planes.

3.3 Anisotropy of swelling

Damp specimens were prepared in the humidifier at 99% relative humidity with the specimen water content increasing in an approximately linear manner; see Fig. 4(a), where we have show measurements of the temporal variation of $\overline{m}$ (the error bars indicate the scatter over 3 nominally identical specimens). The steady-state nominal swelling strains ε_0 of the foam are plotted in Fig. 4(b) as a function of $\overline{m}$ with the error bars again indicating the scatter over 3 nominally identical specimens. The swelling strain is plotted in the R, L and W directions and is highly anisotropic in nature. Upon comparing Figs. 3(b) and 4(b) it is clear that the ranking of swelling strain and strength are inversely correlated: the R direction is the weakest but is also the direction of largest swelling. We proceed to focus attention on the compressive response in the R-direction.

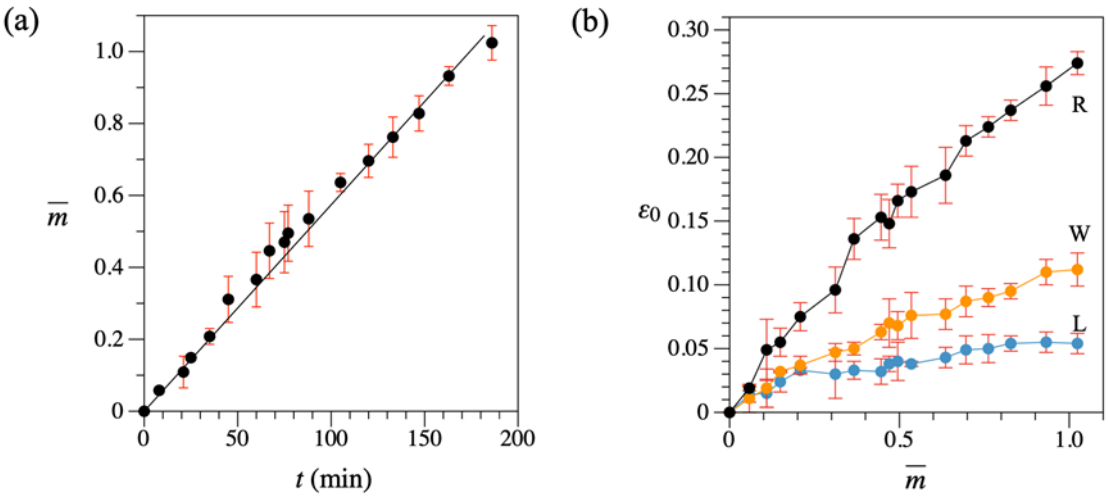

Fig. 4: The swelling response of the dry pre-expanded cellular foam. (a) Temporal evolution of the non-dimensional water content $\overline{m}$ of a specimen placed in a humidity chamber at a relative humidity of 99%. (b) The steady-state swelling strain in the L, R and W directions as a function of $\overline{m}$.

3.4 Strain-rate sensitivity for the damp case, $\bar{m} = 1$

The strain-rate sensitivity of the compressive response of the dry pre-expanded foam ($\bar{m} = 0$) and of the damp foam ($\bar{m} = 1$) was determined by performing tests[2] at a nominal strain rate of 10^{-2} s^{-1}, 10^{-3} s^{-1} and 10^{-4} s^{-1}. The measured nominal stress σ_n versus strain responses are given in Figs. 5(a) and 5(b) for $\bar{m} = 0$ and $\bar{m} = 1$, respectively. For the $\bar{m} = 1$ case we introduce a shifted strain $\hat{\varepsilon} = \varepsilon_n - \varepsilon_0^{(R)}$ and plot σ_n versus $\hat{\varepsilon}$ so that the curves in Fig. 5(b) begin at the origin. The issue does not arise for $\bar{m} = 0$ as $\varepsilon_0^{(R)}$=0, that is $\hat{\varepsilon} = \varepsilon_n$.

Now take the strain rate of 10^{-3} s^{-1} as the reference rate and define a strain rate sensitivity factor as $\alpha = \sigma_n(\dot{\varepsilon})/\sigma_n(10^{-3}s^{-1})$ for a nominal strain that is chosen (arbitrarily) to be $|\hat{\varepsilon}| = 0.2$. This strain-rate sensitivity factor is plotted in Fig. 5(c). We conclude that the rate sensitivity is small (α is close to unity) for the damp foam, $\bar{m} = 1$ but is significant for the dry foam, $\bar{m} = 0$. Further, the shape of the compressive stress versus strain response is almost insensitive to strain-rate once the stress has been scaled by the strain-rate sensitivity factor α. To illustrate this, we introduce the scaled stress $\bar{\sigma}_n(\hat{\varepsilon}) = \alpha(\dot{\varepsilon})\sigma_n(\hat{\varepsilon}, \dot{\varepsilon} = 10^{-3}\mathrm{s}^{-1})$ and compare plots of $\bar{\sigma}_n$ versus $\hat{\varepsilon}$ (dashed lines) for $\overline{m} = 0$ and $\overline{m} = 1$, respectively, with the measured responses (solid coloured lines). In both Figs. 5(d) and (e) the scaled stresses $\bar{\sigma}_n$ are in excellent agreement with the measurements at $\dot{\varepsilon} = 10^{-2}\mathrm{s}^{-1}$ and $\dot{\varepsilon} = 10^{-4}\mathrm{s}^{-1}$ implying that the strain-rate sensitivity factor α is sufficient to characterise the rate sensitivity of the compressive stress versus strain response.

[2] Compressive loading led to a negligible loss of water from the damp specimens, such that the change in value of $\bar{m}$ was less than 3% during the test.

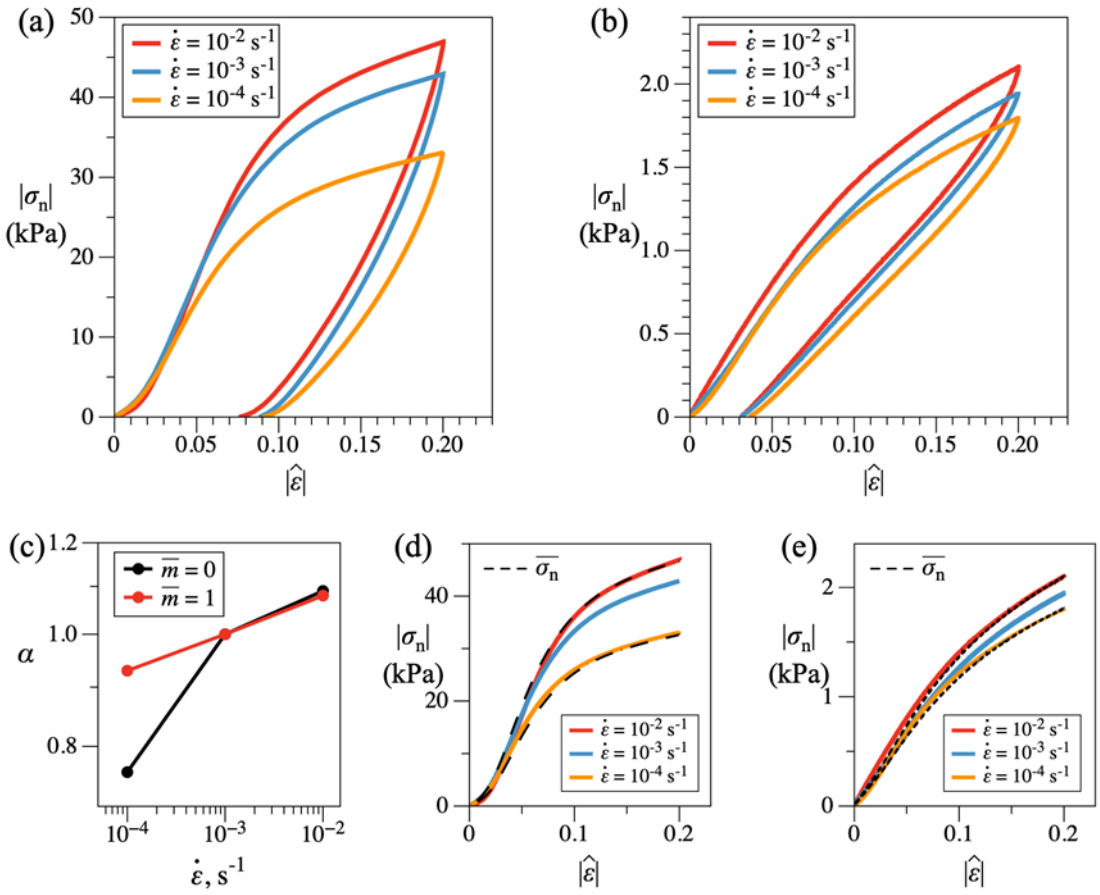

Fig. 5: Effect of strain-rate on compressive stress versus strain responses of the dry and damp cellulose foam. The measured response of the (a) pre-expanded dry ($\overline{m}$ = 0) such that $\hat{\varepsilon} = \varepsilon_n$; and (b) damp foam with $\overline{m}$ = 1. (c) Strain-rate sensitivity α as a function of strain rate $\dot{\varepsilon}$. Comparison between the scaled stress $\bar{\sigma}_n$ and measured stress σ_n as a function of the shifted nominal strain for (d) $\overline{m}$ = 0 and (e) $\overline{m}$ = 1.

3.5 Sensitivity of compressive stress-strain response to water content

A systematic series of compression tests were performed at a nominal strain-rate of 10^{-3}s^{-1}, and at selected values of $\overline{m}$ in the range of 0 to 1.03 to characterise the sensitivity of the compressive response to water content. These results are included in Fig. 6 using axes of nominal stress σ_n and the shifted nominal strain $\hat{\varepsilon} = \varepsilon_n - \varepsilon_0^{(R)}$, where

$\varepsilon_0^{(R)}(\overline{m})$ is the swelling strain for the given value of $\overline{m}$ from Fig. 4(b). In each case, the specimen was compressed to a strain of $\hat{\varepsilon}$ =-0.6 and was then unloaded. The effect of water content upon the compressive response is quantified by introducing a water content sensitivity factor $\beta = \sigma_n(\overline{m})/\sigma_n(0)$ at a compressive strain $\hat{\varepsilon}$ = -0.2, in a manner analogous to the definition of strain-rate sensitivite factor.

The water content sensitivity β is plotted as a function of $\overline{m}$ in Fig. 7(a). In order to explore whether the shape of the stress versus strain curve is invariant with respect to a change in water content, the response at $\overline{m}$ = 0 is scaled by the moiture sensitivity factor β (dashed black lines) by introduction of the scaled stress $\overline{\overline{\sigma_n}}(\hat{\varepsilon}) = \beta(\overline{m})\sigma_n(\hat{\varepsilon}, \overline{m} = 0)$. The scaled stress is compared with the measured curves (solid coloured lines) for $\overline{m}$ > 0 in Fig. 7(b). To a first approximation, the effect of changing the water content is to scale the strength but not change the fundamental shape of the loading portion, and the initial unloading portion, of the stress versus strain curve.

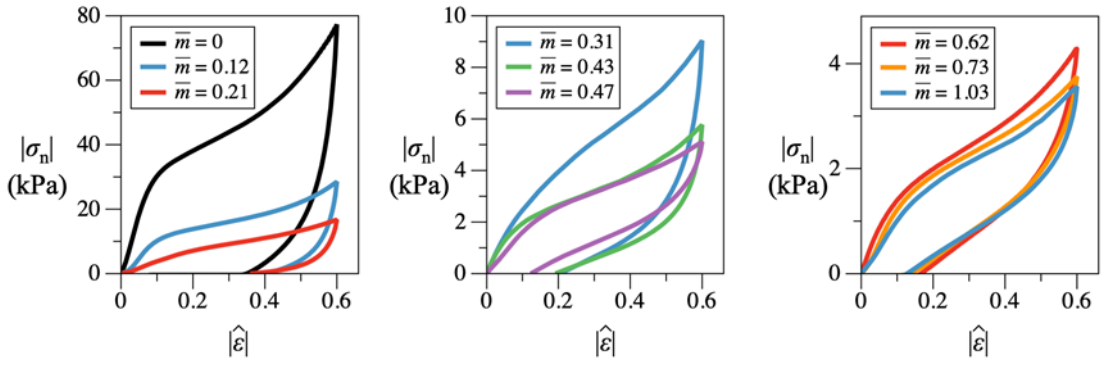

Fig. 6: The compressive responses of the damp foams at a strain rate of 10^{-3} s^{-1}. The three plots show results for water content over the range $0 \leq \overline{m} \leq 1.03$ with the results plotted using axes of the nominal stress σ_n and shifted nominal strain $\hat{\varepsilon} = \varepsilon_n - \varepsilon_0^{(R)}$, where $\varepsilon_0^{(R)}(\overline{m})$ is the swelling strain for the given value of $\overline{m}$ from Fig. 4(b).

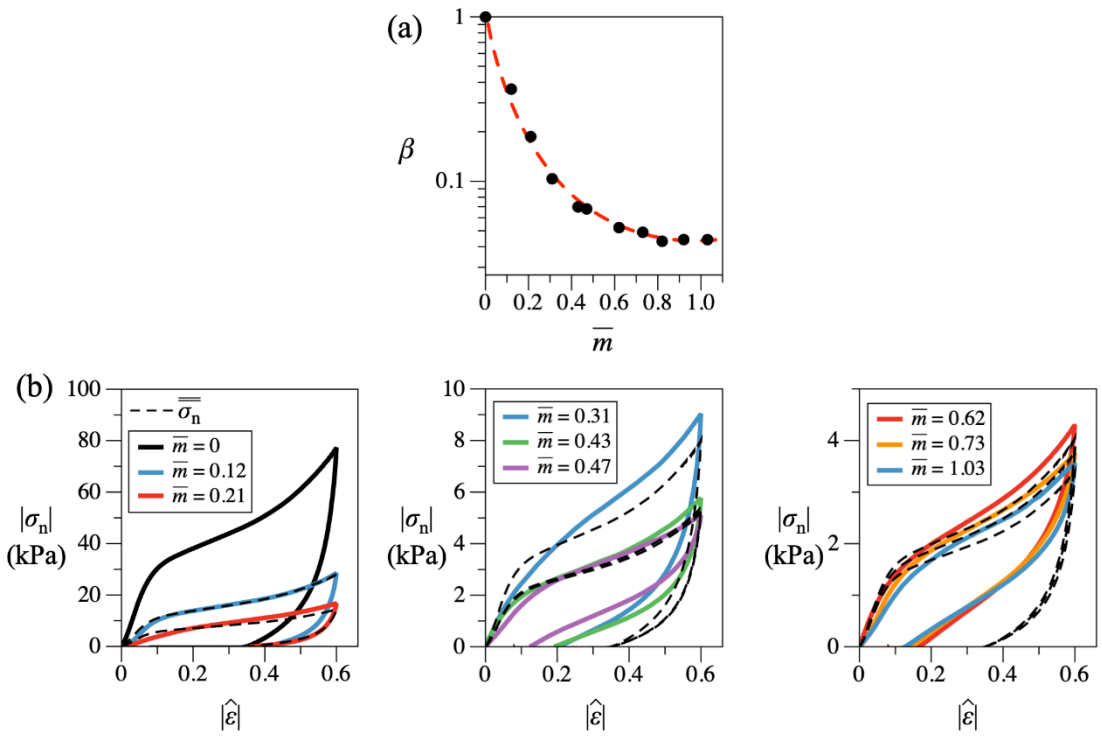

Fig. 7: Effect of water content on the stress versus strain response properties of the foam. (a) The water content sensitivity factor β as a function of $\bar{m}$. (b) Comparison of scaled $\overline{\overline{\sigma_n}}(\hat{\varepsilon})$ and measured stress $\sigma_n(\hat{\varepsilon})$ curves, for water contents in the range $0 \leq \bar{m} \leq 1.03$. The solid, coloured lines are reproduced from Fig. 6.

It is instructive to measure the unloading response of the compression tests in order to give insight into the nature of the hardening response (isotropic versus kinematic). It is clear from Fig. 6 that reverse plasticity occurs upon unloading. The nature of the unloading response is now explored in more detail as follows. First, unload at a value of strain $\hat{\varepsilon} = \hat{\varepsilon}_{max} = -0.6$, see Fig. 8(a). The initial slope of the unloading curve defines a modulus E_U and we associate a plastic strain $\hat{\varepsilon}^p_{max} = \hat{\varepsilon}_{max} - \sigma_n(\hat{\varepsilon} = \hat{\varepsilon}_{max})/E_U$ with the state of the foam at $\hat{\varepsilon} = \hat{\varepsilon}_{max}$. Upon full unloading, there is a permanent residual strain $\hat{\varepsilon} = \hat{\varepsilon}^p$ as defined in Fig. 8(a). The dependence of

$\hat{\varepsilon}^p / \hat{\varepsilon}^p_{max}$ upon $\overline{m}$ is included in Fig. 8(b). Additional tests were performed such that specimens were compressed to $\hat{\varepsilon}_{max} = -0.4$ and then fully unloaded; it is concluded from Fig. 8(b) that the normalised response is almost independent of the choice of $\hat{\varepsilon}_{max}$. A transition in behaviour occurs at $\overline{m}$ = 0.5, as follows. At $\overline{m}$ > 0.5, the ratio $\hat{\varepsilon}^p / \hat{\varepsilon}^p_{max}$ is on the order of 0.3, and is insensitive to the value of $\overline{m}$. For a water content in this regime, the compressive response is also almost insensitive to the strain rate, recall Fig. 7(b). In contrast, for $\overline{m}$< 0.5, the ratio $\varepsilon^p / \varepsilon^p_{max}$ increases with diminishing value of $\overline{m}$ > 0.5, and the compressive response has a higher strain rate sensitivity. For completeness, the dependence of the 0.1% offset yield strength σ_y and the initial Young's modulus E (both defined in Fig. 8a) upon $\overline{m}$ are summarised in Figs. 8(c) and 8(d), respectively. Both the strength and modulus decrease monotonically with increasing $\overline{m}$.

It remains to verify that the response is plastic rather than visco-elastic in nature. We do this by measuring the degree of creep recovery after compression of the foam to a nominal strain $\hat{\varepsilon} = -0.6$ at a strain rate of 10^{-3} s^{-1}, followed by full unloading to zero stress. The temporal variation of $\hat{\varepsilon}$ is included in Fig. 9(a) for specimens of water content $\overline{m}$ =0, 0.54, and 0.96, and time $t = 0$ defined as the instant of unloading to zero stress. The strain has not recovered to zero after 5000 s, which is ten times the duration of the initial loading test. This is further clarified in Fig. 9(b) where we replot the data from Fig. 9(a) normalised by the initial strain at time $t = 0$. For all values of $\overline{m}$ nearly 50% of the initial strain persists after 5000 s. This implies that the compressive response can be considered to be elasto-plastic rather than visco-elastic in nature.

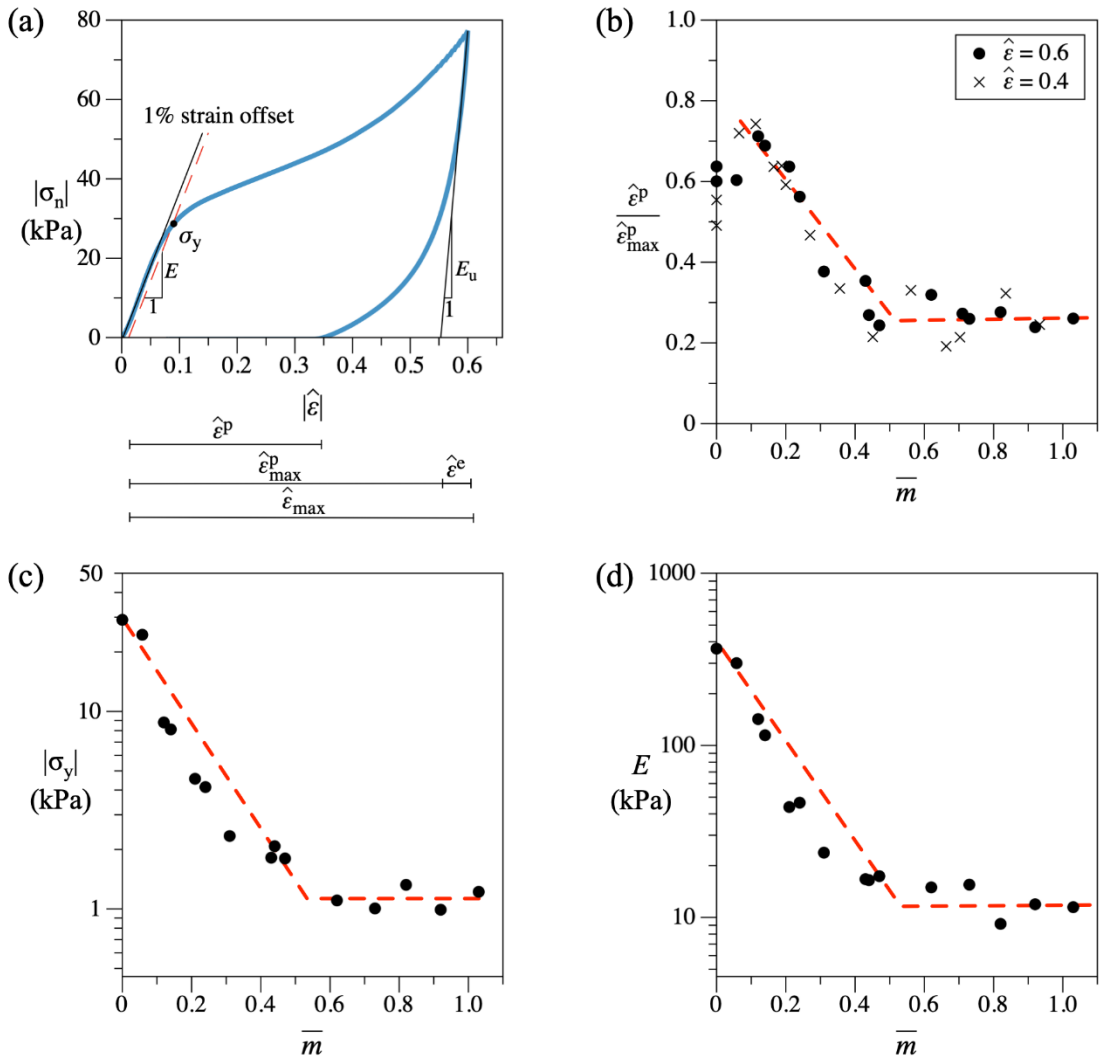

Fig. 8: The effect of water content on the plastic response of the cellulose foam. (a) Definition of the elastic and plastic strains upon loading. (b) The dependence of the residual plastic strain ε^p normalised by the initial plastic strain ε^p_{max} upon water content $\overline{m}$ for unloading from two selected values of ε_{max}. The dependence of (c) compressive yield strength σ_y and (d) initial Young's modulus E upon $\overline{m}$.

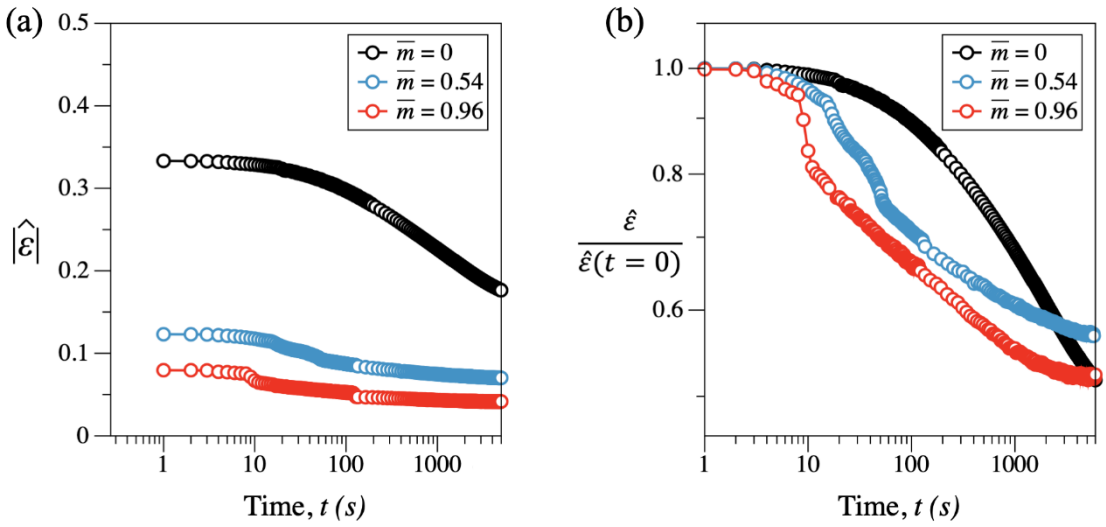

Fig. 9: Creep recovery measurements. (a) Temporal variation of the strain $\hat{\varepsilon}$ upon unloading to zero stress after compression to a nominal strain of $\hat{\varepsilon} = -0.6$. Time $t = 0$ corresponds to the instant of unloading to zero stress. (b) Replot of the data in (a) with $\hat{\varepsilon}$ normalised by its value at $t = 0$.

Finally, the degree of Bauschinger effect is explored by comparing the unloading locus of the stress versus strain curve with the initial forward loading curve. Upon compressing the foam to a prescribed value of $\hat{\varepsilon}$ the sample is unloaded; write $\Delta\sigma_n$ and $\Delta\hat{\varepsilon}$ as the unloading increments in stress and strain, respectively. The aim is to compare the $\Delta\sigma_n$ and $\Delta\hat{\varepsilon}$ response with the σ_n versus $\hat{\varepsilon}$ response. We conducted a loading-unloading compression test (by progressively increasing the loading to $|\hat{\varepsilon}|$ = 0.05, 0.1, 0.2, 0.4, 0.6) on specimens of water content $\overline{m}$= 0, 0.5, and 1, as shown in Fig. 10(a). The reversed, unloading curves ($\Delta\sigma_n$ versus $\Delta\hat{\varepsilon}$) in the fourth and fifth cycles are compared with the forward loading response in Fig. 10(b). A very strong Bauschinger effect exists to the extent that reversed plastic flow occurs at a stress increment $\Delta\sigma_n$ equal to the compressive yield strength rather than twice the compressive yield strength.

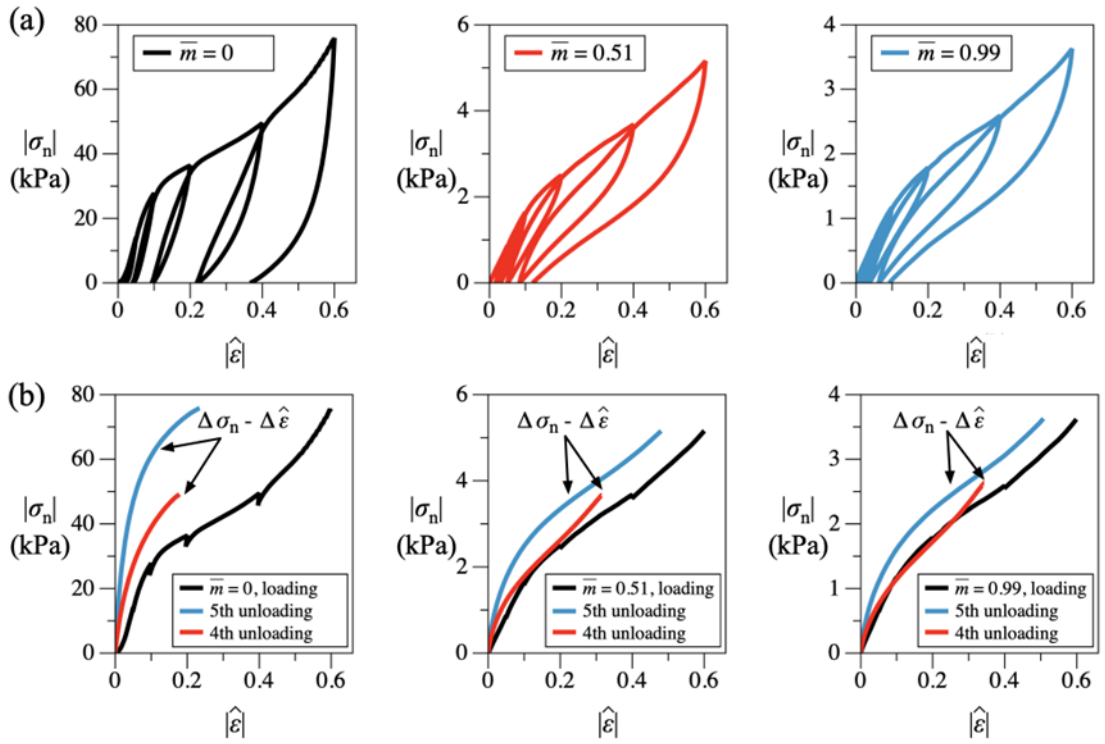

Fig. 10: Investigation of the Bauschinger effect. (a) Loading-unloading compressive response for selected values of of water content in the range $0 \leq \bar{m} < 1$. (b) Comparison of the unloading $\Delta\sigma_n$ versus $\Delta\hat{\varepsilon}$ curves for the 4th and 5th unloadings with the loading compressive response.

4. Conclusions

The effect of water content and deformation rate upon deformation (and actuation) behaviour of a pre-expanded ellulose foam has been measured. Both tensile and compressive responses are reported along with the degree of anisotropy in mechanical properties. The cellulose foam exhibits the lowest strength in the rise direction (R) for both tension and compression. Over the range of strain rate and water content considered, the compressive stress versus strain response of the cellulose foam is adequately approximated by a visco-plastic, transversely isotropic, compressible material model. To

first order, the shape of the stress versus strain curve is insensitive to the strain rate and water content, but the magnitude of stress is amplified by a multiplying factor that depends upon strain rate and water content. Intriguingly, reversed plastic flow is initiated upon unloading from the plastic state by a stress increment equal to the initial yield stress. This is example of an extreme form of kinematic hardening.

Declaration of competing interest

The authors declare that they have no known competing financial interests or personal relationships that could have appeared to influence the work reported in this paper.

Acknowledgements

This work was supported by the European Research Council (ERC) in the form of advanced grant, MULTILAT, GA669764. The authors are grateful to Sri Datta, Ratul Das, and Joe Stallard of Cambridge University Engineering Department for the design and discussion of the experiments.

References

Ashby, M.F., Evans, A.G., Fleck, N.A., Hutchinson, J.W. , Wadley, H.N.G., Gibson, L.J., 2000. Metal foams: a design guide. Elsevier.

Ashby, M.F., Gibson, L.J., 1997. Cellular solids: structure and properties. Press Syndicate of the University of Cambridge, Cambridge, UK, 175-231.

Chen, P., Wohlert, J., Berglund, L., Furó, I., 2022. Water as an intrinsic structural element in cellulose fibril aggregates. The Journal of Physical Chemistry Letters 13, 5424-5430.

Das, R., Deshpande, V.S., Fleck, N.A., 2022. The transport of water in a cellulose foam. Extreme Mechanics Letters, 101897.

Deshpande, V.S., Fleck, N.A., 2000. Isotropic constitutive models for metallic foams. Journal of the Mechanics and Physics of Solids 48, 1253-1283.

Deshpande, V.S., Fleck, N.A., 2001. Multi-axial yield behaviour of polymer foams. Acta materialia 49, 1859-1866.

Dinwoodie, J.M., 2000. Timber: its nature and behaviour. CRC Press.

Fleck, N.A., Deshpande, V.S., Ashby, M.F., 2010. Micro-architectured materials: past, present and future. Proceedings of the Royal Society A: Mathematical, Physical and Engineering Sciences 466, 2495-2516.

Ha, J., Kim, J., Jung, Y., Yun, G., Kim, D.-N., Kim, H.-Y., 2018. Poro-elasto-capillary wicking of cellulose sponges. Science advances 4, eaao7051.

KADLA, J.F., GILBERT, R.D., 2000. Cellulose structure: A review. Cellulose Chemistry and Technology 34, 197-216.

Kim, J., Ha, J., Kim, H.-Y., 2017. Capillary rise of non-aqueous liquids in cellulose sponges. Journal of Fluid Mechanics 818.

Lin, N., Dufresne, A., 2014. Nanocellulose in biomedicine: Current status and future prospect. European Polymer Journal 59, 302-325.

Lv, P., Lu, X., Wang, L., Feng, W., 2021. Nanocellulose ‐ based functional materials: from chiral photonics to soft actuator and energy storage. Advanced Functional Materials 31, 2104991.

Mirzajanzadeh, M., Deshpande, V.S., Fleck, N.A., 2019. Water rise in a cellulose foam: By capillary or diffusional flow? Journal of the Mechanics and Physics of Solids 124,

206-219.

Mirzajanzadeh, M., Deshpande, V.S., Fleck, N.A., 2020. The swelling of cellulose foams due to liquid transport. Journal of the Mechanics and Physics of Solids 136, 103707.

Nan, M., Wang, F., Kim, S., Li, H., Jin, Z., Bang, D., Kim, C.-S., Park, J.-O., Choi, E., 2019. Ecofriendly high-performance ionic soft actuators based on graphene-mediated cellulose acetate. Sensors and Actuators B: Chemical 301, 127127.

Sinko, R., Keten, S., 2014. Effect of moisture on the traction-separation behavior of cellulose nanocrystal interfaces. Applied Physics Letters 105, 243702.

Tankasala, H.C., Li, T., Seiler, P.E., Deshpande, V.S., Fleck, N.A., 2020. An assessment of the J-integral test for a metallic foam. Journal of the Mechanics and Physics of Solids, 141, 103958.

Tagarielli, V.L, Deshpande, V.S., Fleck, N.A. and Chen, C., 2005. A constitutive model for transversely isotropic foams, and its application to the indentation of balsa wood, International Journal of Mechanical Sciences, 47(4-5), 666-686.

Tjahjanto, D.D., Girlanda, O., Östlund, S., 2015. Anisotropic viscoelastic–viscoplastic continuum model for high-density cellulose-based materials. Journal of the Mechanics and Physics of Solids 84, 1-20.

Yamamoto, H., Sassus, F., Ninomiya, M., Gril, J., 2001. A model of anisotropic swelling and shrinking process of wood. Wood Science and Technology 35, 167-181.

Zhu, Q., Jin, Y., Wang, W., Sun, G., Wang, D., 2018. Bioinspired smart moisture actuators based on nanoscale cellulose materials and porous, hydrophilic EVOH nanofibrous membranes. ACS applied materials & interfaces 11, 1440-1448.

Zhou, Y., Ren, L., Zang, J., Zhang, Z., 2022. The Shape Memory Properties and Actuation Performances of 4D Printing Poly (Ether-Ether-Ketone). Polymers 14, 3800.